Resource partitioning and amino acid assimilation in a terrestrial geothermal spring

Dengxun Lai, Brian P. Hedlund, Rebecca L. Mau, Jian-Yu Jiao, Junhui Li, Michaela Hayer, Paul Dijkstra, Egbert Schwartz, Wen-Jun Li, Hailiang Dong, Marike Palmer, Jeremy A. Dodsworth, En-Min Zhou, Bruce A. Hungate

Supplementary Tables

Supplementary Figures

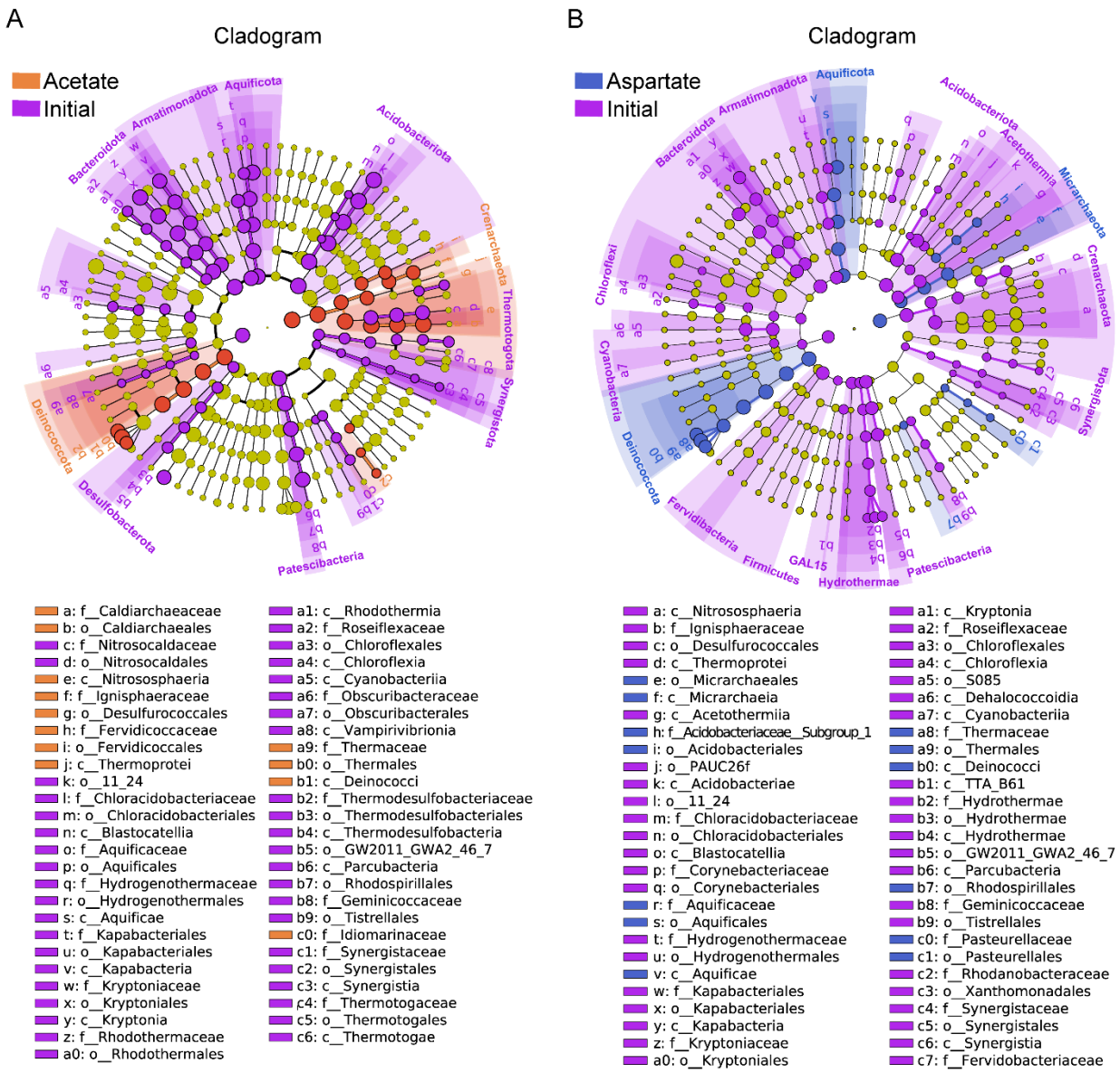

Figure S1. Linear discriminative analysis effect size (LEfSe) of microbial abundance at multiple taxonomic levels with ^{13}C-acetate and ^{13}C-aspartate incubations. (A) Cladogram represents the taxa that were more abundant in the initial samples (purple) and samples incubated with ^{13}C-acetate (orange). Yellow nodes represent taxa with no significant change in abundance during incubations. (B) Cladogram represents the taxa that were more abundant in the initial samples (purple) and samples incubated with ^{13}C-aspartate (blue).

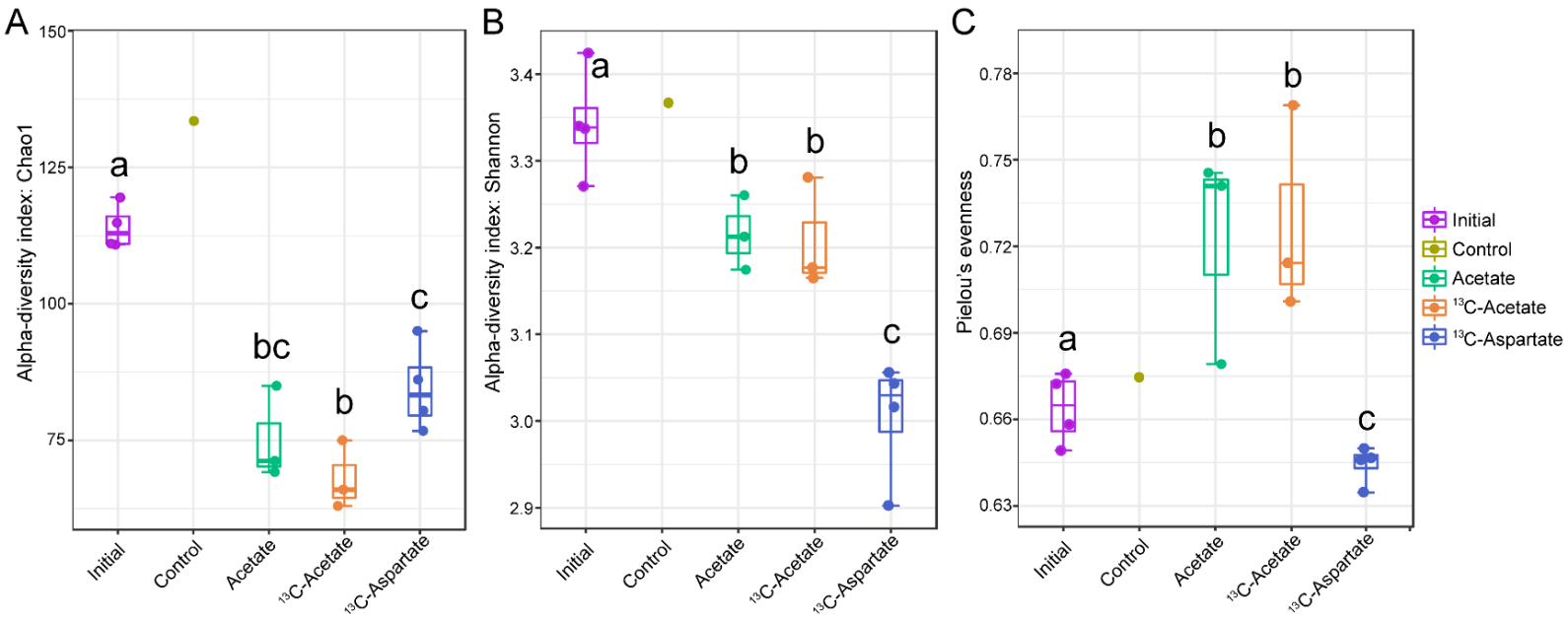

Figure S2. Effect of incubation on alpha diversity. Microbial alpha diversity as assessed with the Chao1 index (A), Shannon diversity index (B) and Pielou's Evenness (C) in the five groups: initial (purple), control (brown), natural abundance acetate (green), ^{13}C-acetate (orange), and ^{13}C-aspartate (blue). The same lowercase letter indicates no significant difference based on Welch's t-test ($p > 0.05$). The analysis shows that incubation with any substrate significantly reduced both richness and Shannon diversity (versus initial).

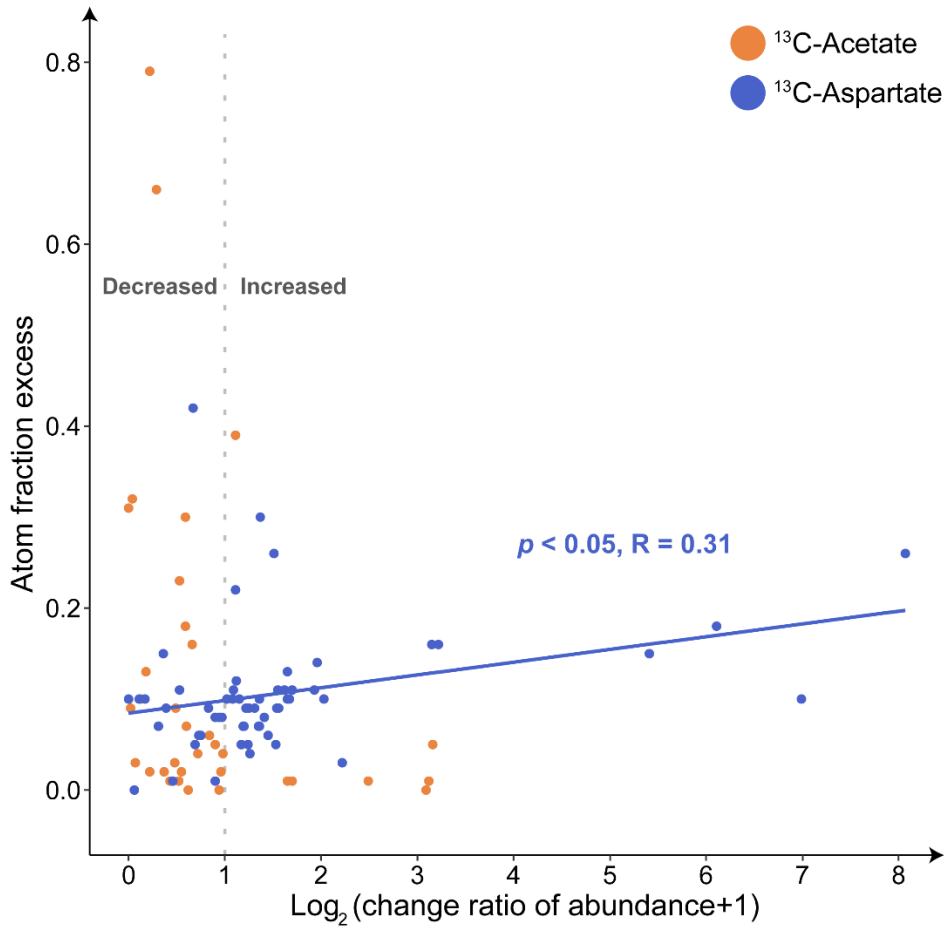

Figure S3. Aspartate enhances the growth of some taxa. Association between the change ratio of absolute abundance and AFE of ^{13}C-acetate (orange) and ^{13}C-aspartate (blue). The statistical significance of the relationships was based on Pearson correlation coefficient test.

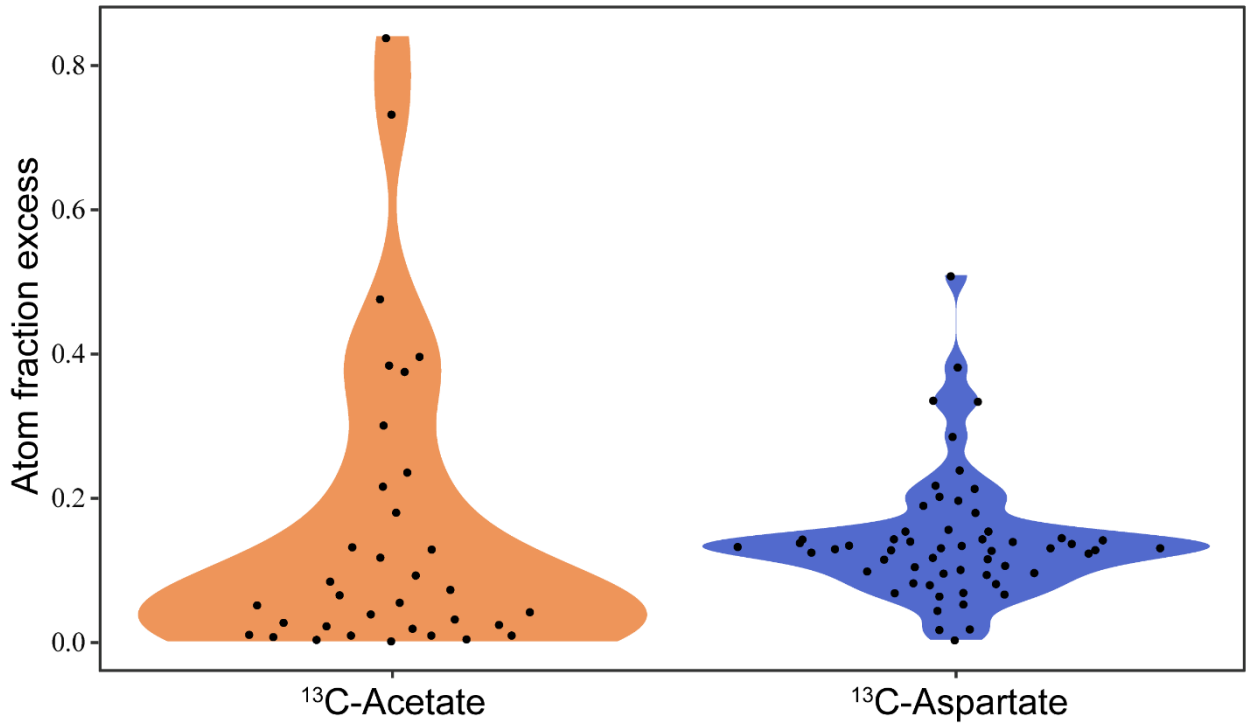

Figure S4. Distribution of atom fraction excess values among ASVs. ASVs enriched with ^{13}C-acetate (orange) or ^{13}C-aspartate (blue), which are not significantly different (Asymptotic General Independence Test, $p = 0.499$).

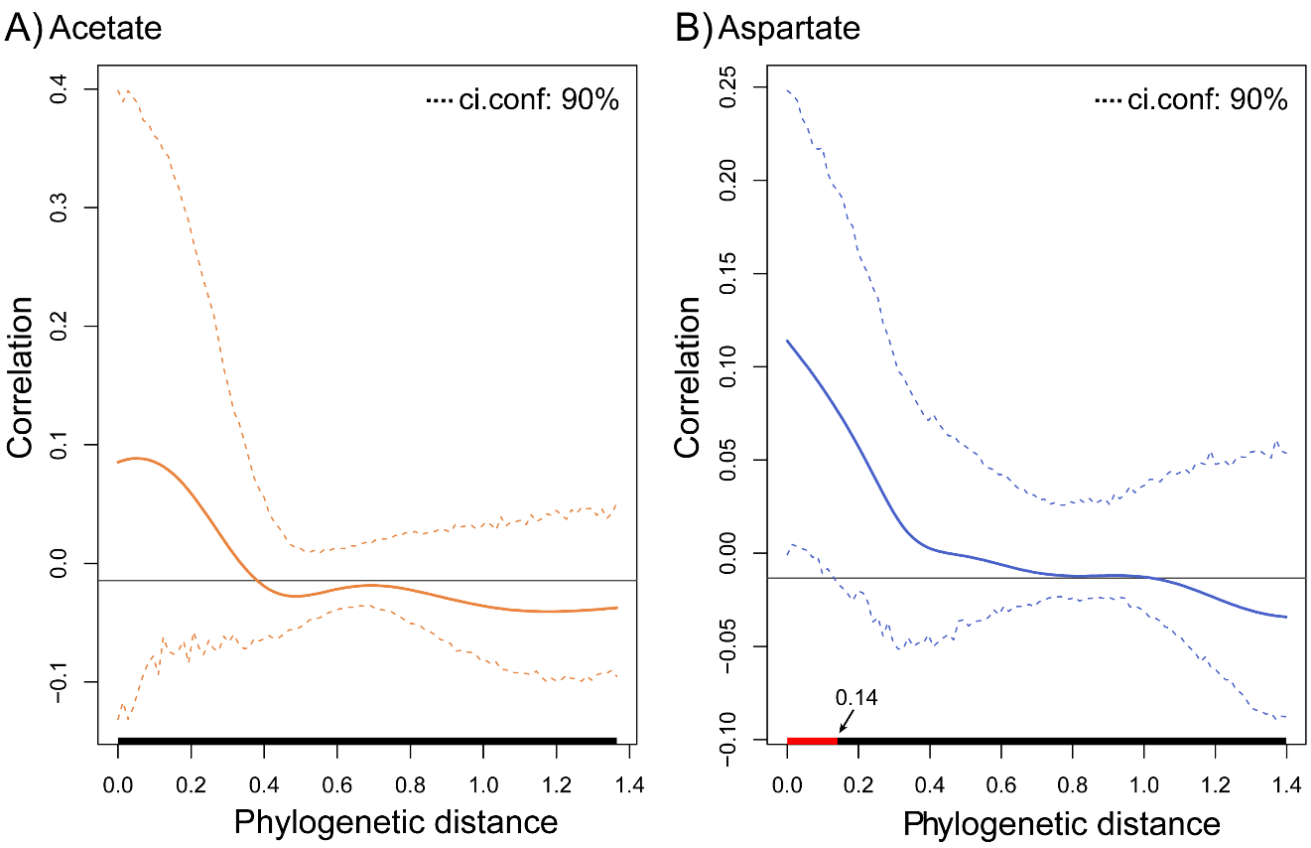

Figure S5. Aspartate utilization shows a positive phylogenetic autocorrelation across short phylogenetic distances (low taxonomic rank). Phylogenetic correlograms for acetate (orange) and aspartate (blue) datasets. Moran's I autocorrelation is represented by the solid line, and the lower and upper bounds of the 90% confidence interval, which was computed using nonparametric bootstrap resampling are shown by the dashed lines. The horizontal black line represents the expected Moran's I values under the null hypothesis of no phylogenetic autocorrelation. Red shown on the x-axis indicates a significant positive autocorrelation and black indicates no autocorrelation. There was no significant autocorrelation above 0.14 phylogenetic distance for aspartate utilization.

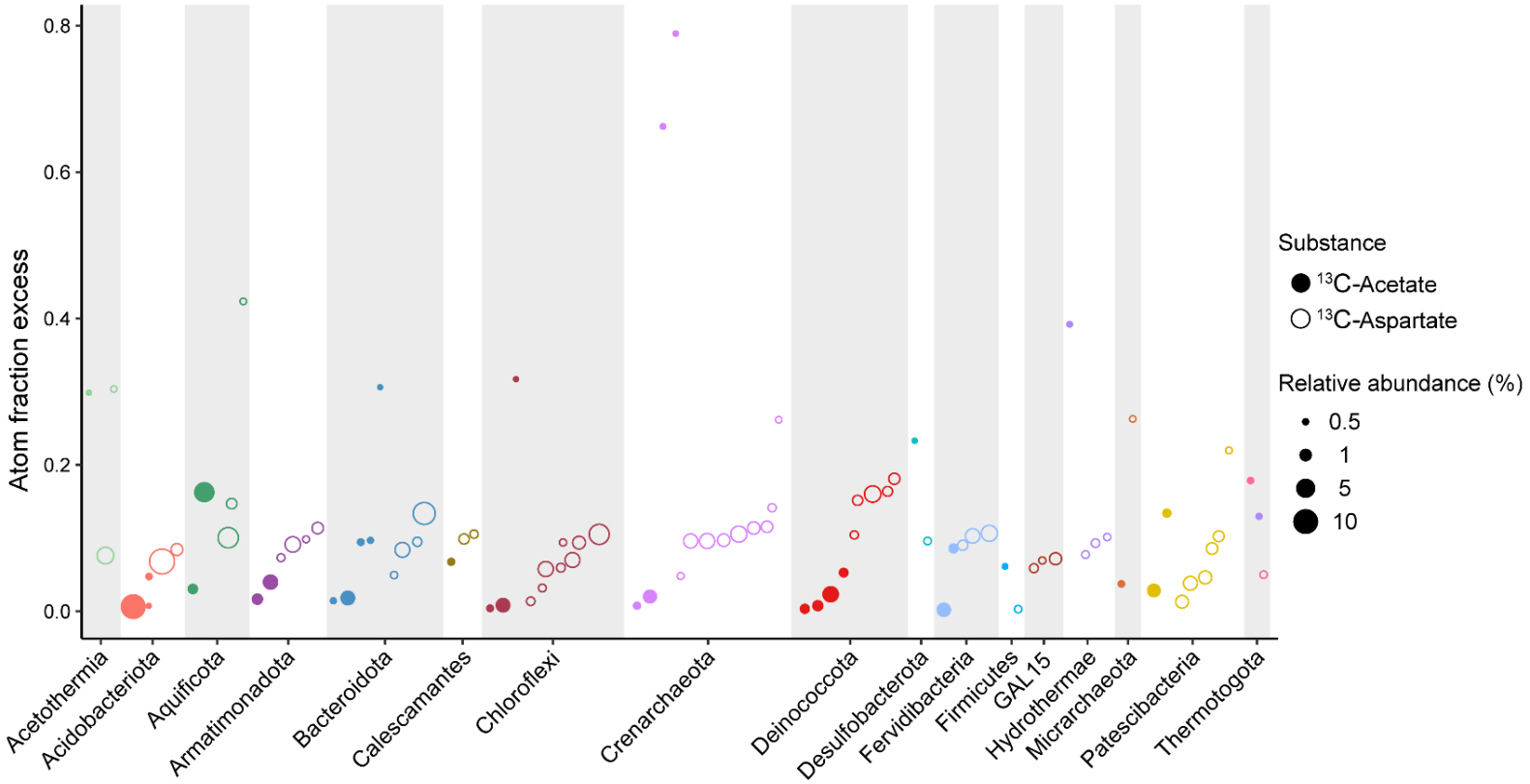

Figure S6. High activity of rare taxa. Scatter plot showing atom fraction excess of ^{13}C after incubation with ^{13}C-acetate (solid circle) or ^{13}C-aspartate (hollow circle) in ASVs belonging to different phyla. Dot size represents average relative abundance in initial samples (time 0). For both substrates, the most active taxa are rare (<0.5 %). Refer to Supplemental Table 3 for detailed information about ASVs used in the figure.

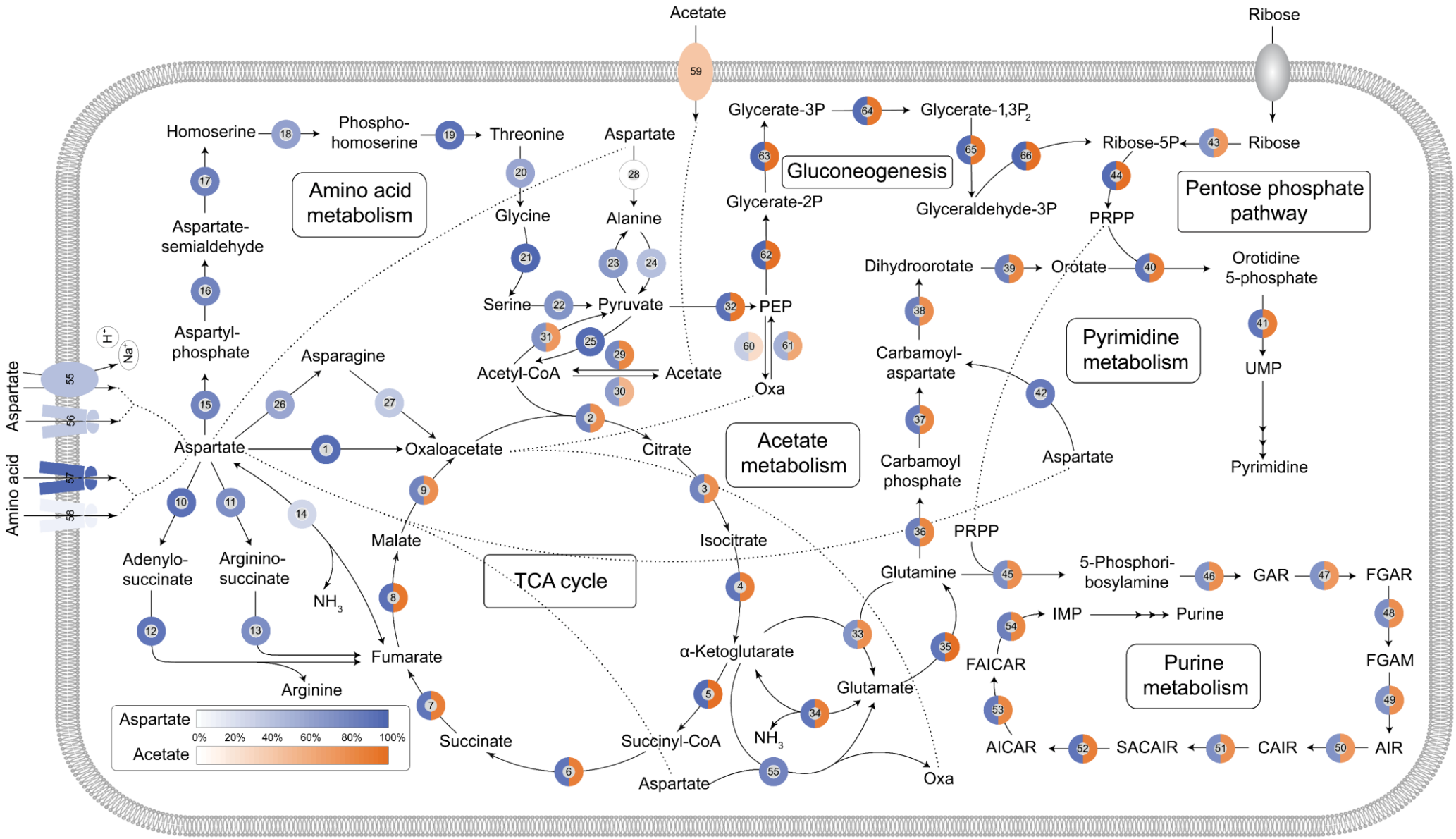
Acetate
Ribose
Homoserine
Phospho-homoserine
Threonine
Aspartate
Amino acid metabolism
Aspartate-semialdehyde
Aspartyl-phosphate
Glycine
Alanine
Serine
Pyruvate
PEP
Acetyl-CoA
Acetate
Oxa
Asparagine
Aspartate
Oxaloacetate
Citrate
Acetate metabolism
Malate
Isocitrate
TCA cycle
Adenylo-succinate
Arginino-succinate
NH3
Fumarate
Arginine
α-Ketoglutarate
Glutamate
Succinate
Succinyl-CoA
NH3
Aspartate
Oxa
Glycerate-3P
Glycerate-1,3P2
Gluconeogenesis
Glycerate-2P
Glyceraldehyde-3P
Ribose-5P
Ribose
Pentose phosphate pathway
PRPP
Dihydroorotate
Orotate
Orotidine 5-phosphate
Pyrimidine metabolism
Carbamoyl-aspartate
UMP
Carbamoyl phosphate
Aspartate
Pyrimidine
PRPP
Glutamine
5-Phosphori-bosylamine
GAR
FGAR
IMP
Purine
FAICAR
Purine metabolism
FGAM
AICAR
SACAIR
CAIR
AIR
Aspartate
Amino acid
H+
Na+
0%
20%
40%
60%
80%
100%
Aspartate
Acetate

Figure S7. Metabolic pathways showing the incorporation of aspartate and acetate into nucleotides. 32 high-quality genomes (>90% completeness and <5% contamination) matched to the ASVs showing aspartate utilization and 19 high-quality genomes matched to ASVs showing acetate utilization were screened. The shades of color represent the proportion of genes detected in the genomes. The map indicates the incorporation of aspartate and acetate into nucleotides is feasible.

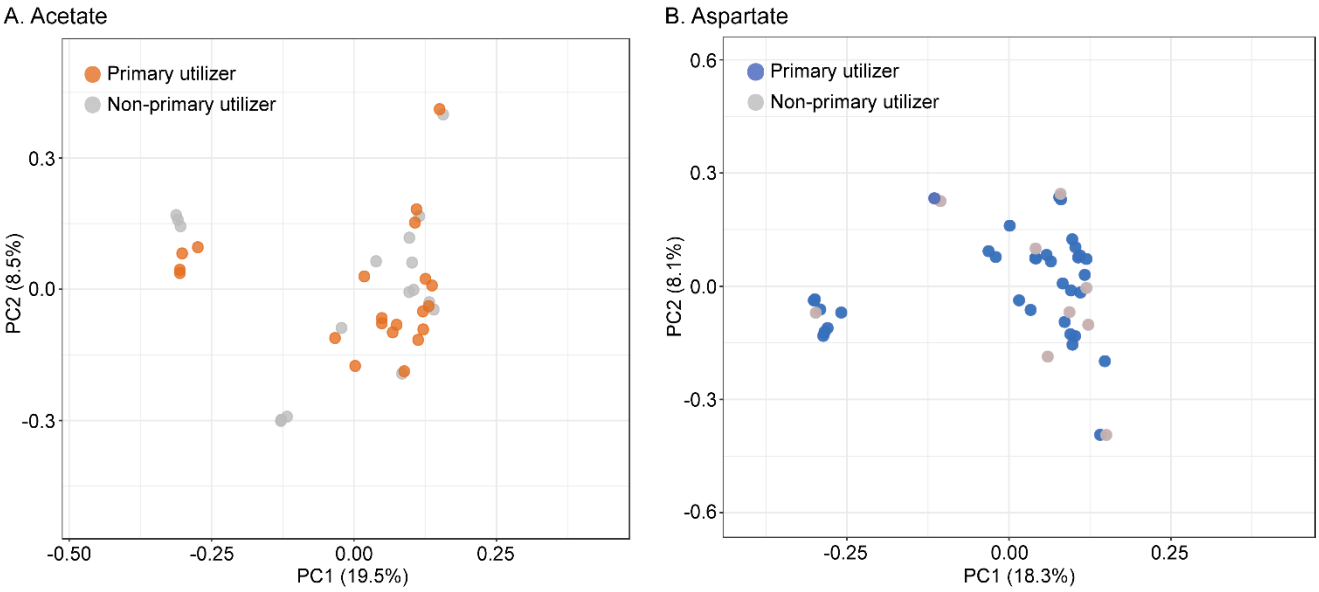

Figure S8. Similar gene content in (A) acetate primary utilizers and non-primary utilizers and (B) aspartate primary utilizers and non-primary utilizers. Principal coordinates analysis (PCoA) plot with Bray-Curtis dissimilarity based on the functional profiling of genomes annotated by KEGG (Supplemental table 4).

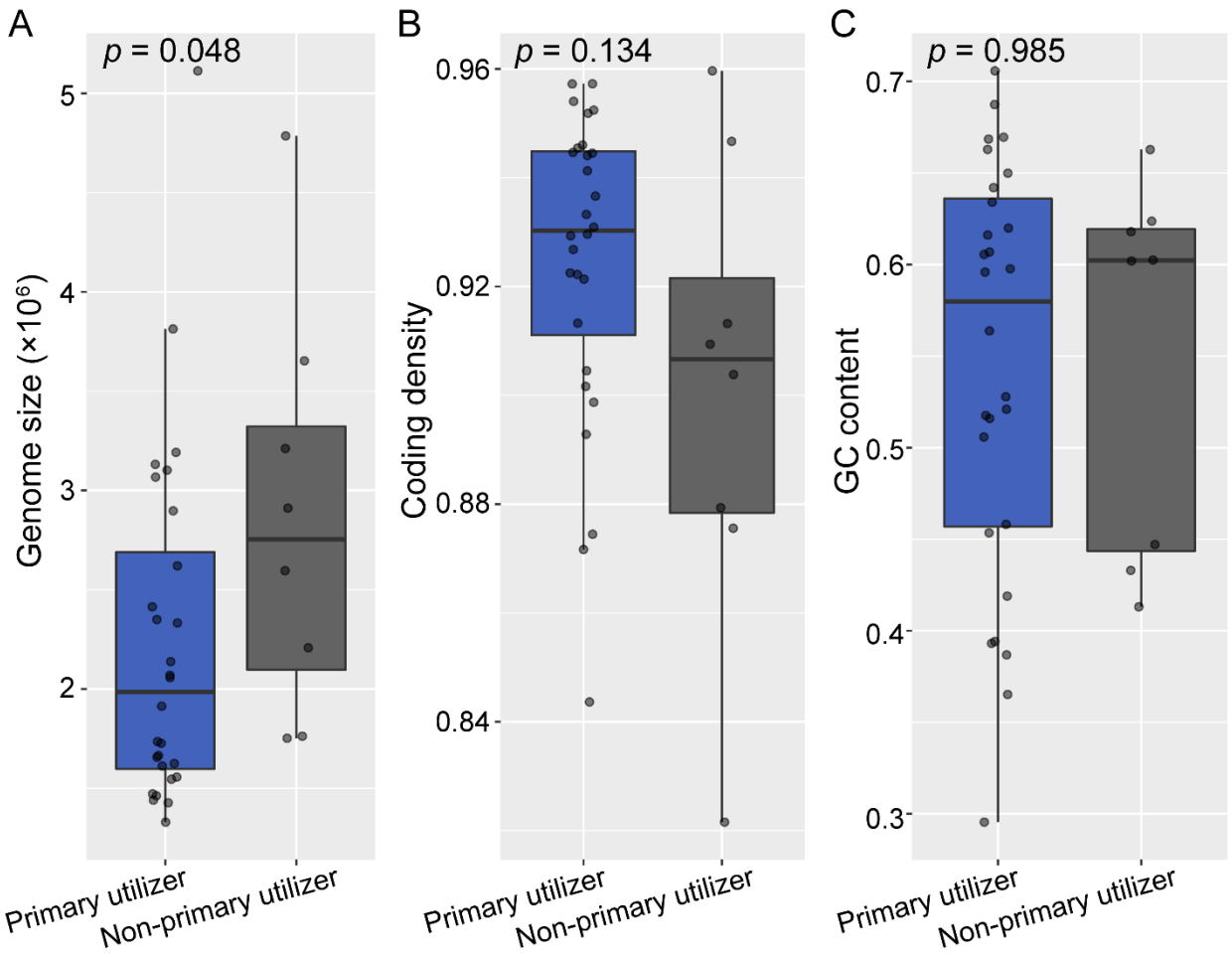

Figure S9. Smaller genome and higher coding density in genomes of aspartate-primary utilizers. Boxplot comparison of (A) genome size, (B) coding density and (C) GC content between aspartate-primary utilizers (blue) and non-primary utilizers (grey). Statistical significance was measured by Wilcoxon exact rank sum test.

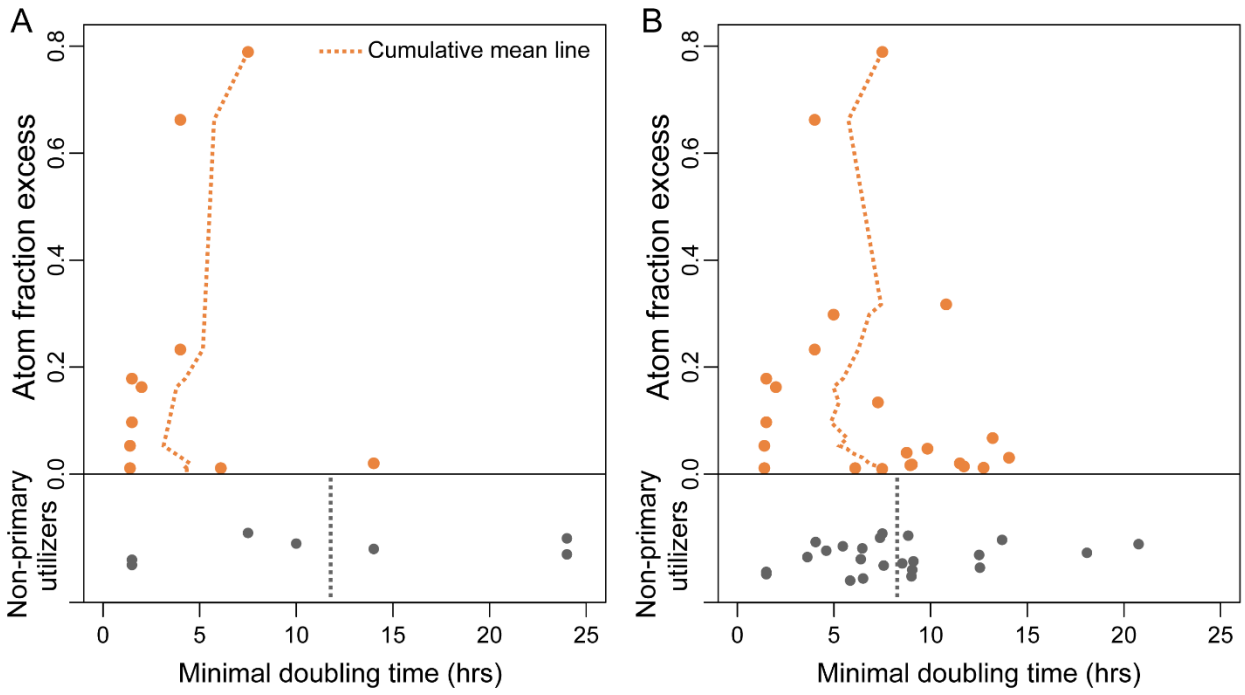

Figure S10. Acetate utilization does not correspond to maximum growth rate. Scatter plots showing the acetate AFE values and minimal doubling time (A) based on literature or (B) literature and gRodon2 estimations. The dashed line represents the cumulative mean line.

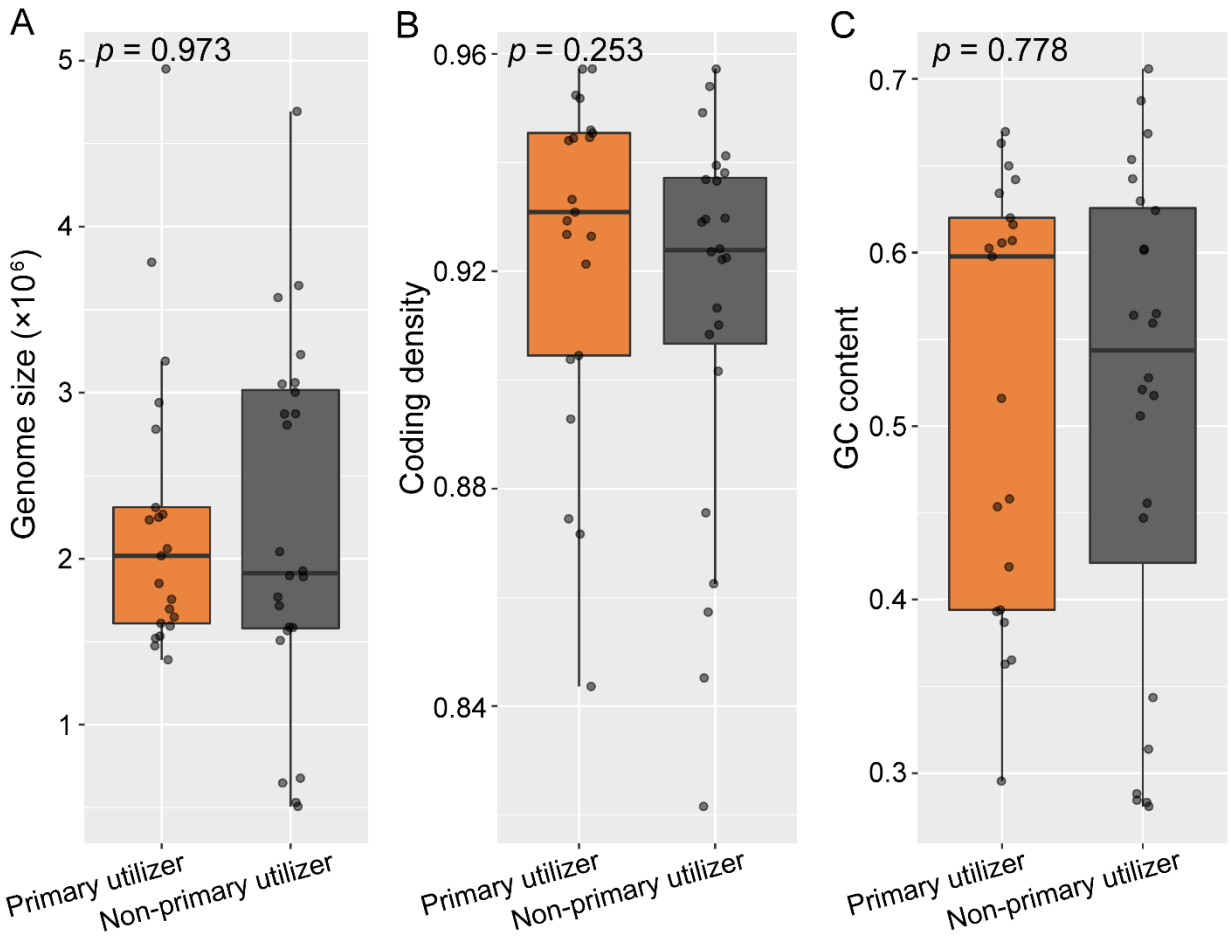

Figure S11. No significant differences in genome size, coding density, and GC content in genomes of acetate-primary utilizers. Boxplot comparison of (A) genome size, (B) coding density, and (C) GC content between acetate-primary utilizers (blue) and non-primary utilizers (grey). Statistical significance was measured by Wilcoxon exact rank sum test.